11th U. S. National Combustion Meeting
Organized by the Western States Section of the Combustion Institute
March 24–27, 2019
Pasadena, California

The Effect of Working Fluids on Premixed Hydrogen Combustion in a Constant Volume Combustion Chamber

Mohammadrasool Morovatiyan[1,], Martia Shahsavan[1], Jonathan Aguilar[1], John Hunter Mack[1]*

[1]Department of Mechanical Engineering, University of Massachusetts Lowell
[1]One University Ave, Lowell, MA, USA
[*]Corresponding Author Email: Mohammadrasool_Morovatiyan@uml.edu

Abstract: Premixed combustion of hydrogen was investigated with the purpose of examining the effect of the full or partial substitution of argon for nitrogen in air on laminar burning velocity. Theoretically, this partial replacement decreases the NOx emissions and increases the thermal efficiency of internal combustion engines due to the high specific heat ratio of noble gases. An optically-accessible constant volume combustion chamber (CVCC) with central ignition was used to study flame propagation, flame morphological structure, and instability. The spherical flame development was studied using a high-speed Z-type Schlieren visualization system. Moreover, a numerical model was developed to convert the pressure rise data to laminar burning velocity. Coupling the model to a chemical equilibrium code aids in determining the burned gas properties. The experimental and numerical investigations indicate that increasing the concentration of argon as the working fluid in the mixture can increase the laminar burning velocity and extend the lean flammability limit.

Keywords: Premixed Hydrogen Combustion, Laminar Burning Velocity, Argon, Constant Volume Combustion Chamber, Z-type Schlieren visualization system

1. Introduction

Efficiencies and emissions are two significant aspects of internal combustion (IC) engines that have been extensively studied over the several decades. Engine performance depends on several parameters including fuel type [1-5], working fluid [6-8], ignition modifications [9-11], and injection techniques [12-15]. Unlike hydrocarbon fuels, hydrogen can potentially decrease emissions while increasing the efficiency of IC engines. Moreover, replacing nitrogen with argon as the working fluid theoretically aids in decreasing NOx production and increasing the thermal efficiency due to the high specific heat ratio of noble gases.

Laminar burning velocity, a fundamental phenomenon in premixed combustion, plays a key role in understanding a mixture's reactivity, diffusivity, and exothermicity [16-18]. It is used in turbulent combustion models to study the turbulent flame propagation, emissions production, and flame morphological structure and instability. Moreover, many chemical kinetics models are validated by laminar burning velocity. Keck [19, 20] studied turbulent flame structure and speed by applying laminar burning velocity on his model validated for spark-ignited IC engines. Menon et al [21] developed a turbulent model that incorporated laminar burning velocity to investigate the wrinkled region of turbulent premixed combustion. Shy et al [22] conducted an experimental

study to propose a premixed turbulent combustion model that predicts flame stretch and quenching.

In this study, the effect of full and partial substitution of argon for nitrogen on premixed hydrogen combustion and its spherically expanding premixed flames in a constant volume combustion chamber (CVCC) is examined. In the experiments, the oxidizer ratio (21%) is kept constant. The laminar burning velocity of H_2-O_2-N_2/Ar mixture has been quantified at three different volumetric percentage of argon in N_2-Ar mixture (0%, 50%, and 100%) at a range of initial pressures (from 0.2 to 0.6 atm) at a constant initial temperature (298 K) and a wide range of equivalence ratios (0.2-3). The effect of increasing the argon concentration shows a positive dependency on the laminar burning velocity, along with extending the lean flammability limit of hydrogen at an initial pressure of 0.2 bar. Moreover, the morphological structures of H_2-O_2-N_2/Ar premixed flames have been studied during flame propagation.

2. Methods

2.1 Experimental Facilities

A constant volume combustion chamber (CVCC), seen in Figure 1, is used to study flame propagation, flame morphological structure, and instability. The pressure rise is measured for each combustion event. The 1.93 liter stainless steel CVCC is a cylindrical chamber with an internal diameter and length of 135 mm. To provide visual access to the combustion process, two 50.8 mm thick quartz windows are supplied at both ends of the CVCC and supported by two flanges. The optically-accessible chamber is sealed using nitrile rubber elastomer O-rings between the quartz windows and the flanges. A Kistler 601CAA high precision water-cooled piezoelectric pressure transducer with a Kistler 5018B charge amplifier are used to measure the dynamic pressure rise. In addition, the chamber is equipped with a K-type thermocouple (Omega KMTXL-062G-6) for measuring the initial gas temperature, a gas inlet/outlet, and two extended spark plugs. The spark plugs with extended 2.5 mm diameter electrodes are installed on the chamber at opposite sides to make a spark gap of 1.2 mm in the center of the chamber.

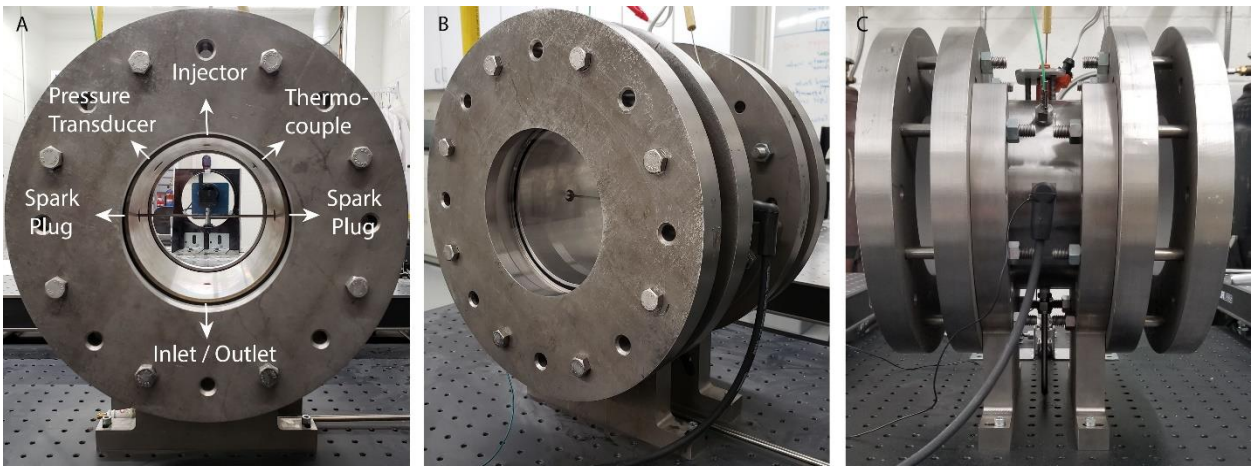

Figure 1: Optical constant volume combustion chamber in (A) Side view, (B) Isometric view, (C) Front view

In the interest of observing flame propagation and morphological structures, a Z-type Schlieren ensemble is utilized with a high-speed high-resolution CMOS camera (Edgertronic SC2+), accompanied with a light source with a 1 mm pin hole, two concave mirrors with internal diameters of 152.4 mm, and a knife edge. The high-speed camera captures images with a rate of up to 31,191 frames per second that is optimized depending on flame burning velocity. The camera supports an exposure range from 1/30 to 1/800,000 second that is optimized regarding the image brightness. By passing through a condensing lens, the light emitted from the light source are collected in the pin hole which is placed at the focal length of the first mirror (1524 mm). The parallel beams between the mirrors are finally collected at the knife edge that is located at the focal length of the second mirror (1524 mm).

Figure 2 shows a schematic diagram of the experimental ensemble. The gas delivery system is connected to a pressure control unit with three high accuracy pressure transducers (Omega PX419 type) optimized for different ranges. A data acquisition system (National Instruments LabVIEW) is used to collect data and synchronize all electrical instruments including ignition system and camera.

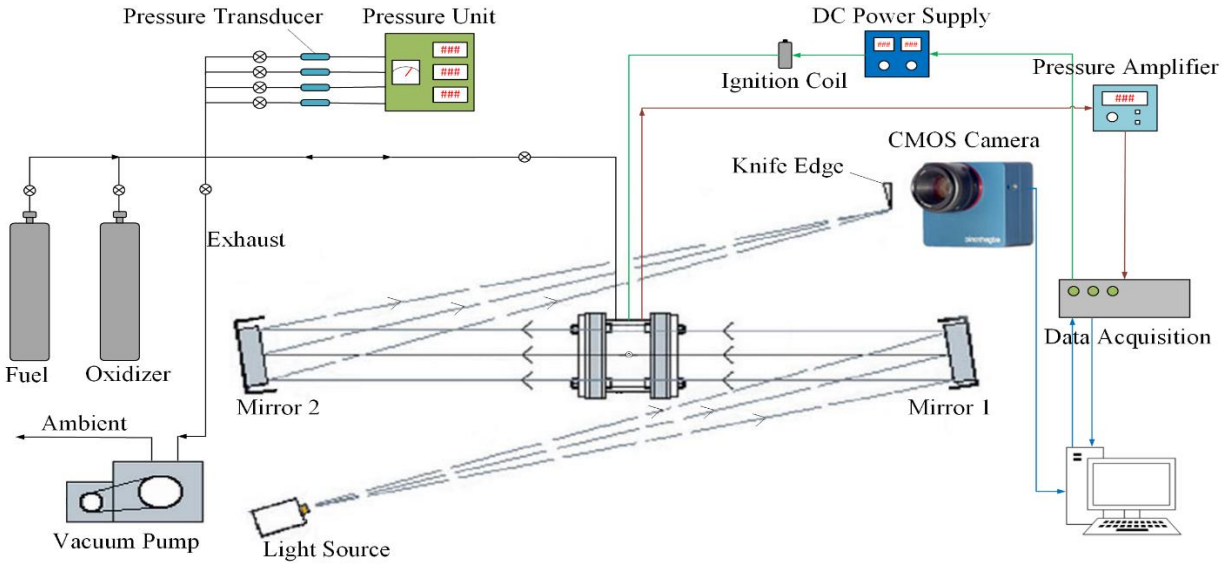

Figure 2: Schematic diagram of experimental systems

2.2 Experimental Procedures

A partial pressure method is employed to fill the optical chamber with expected gaseous mixture utilizing the gas delivery system including valves, pipes, pressure transducers, gas bottles, and vacuum pump. To calculate the partial pressures of each reactant for an equivalence ratio and an initial pressure, a MATLAB script has been written based on the ideal gas law, considering a global chemical reaction for fuel-oxidizer-diluent mixture and atomic balance. In the ideal gas law, the partial pressure is defined in terms of molar fraction of each gas in the mixture. The experimental procedure begins by vacuuming the CVCC and the gas delivery system to a pressure less than 400 mTorr to ensure the vessel is empty of residual gases that potentially effect on the results. The chamber is filled with the mixture and is allowed 5 minutes to reach a steady state. This is sufficient to have a uniform well-mixed mixture and temperature. The spark plug is then triggered and a flame kernel is generated in center of the chamber; the flame front then propagates spherically through the chamber.

2.3 Laminar Burning Velocity Measurement

In order to calculate the laminar burning velocity, a numerical model is used by considering the pressure rise data in the CVCC. The pressure-time data should be evaluated for the region that flame front is laminar and unstretched. Since the premixed flame expands in the chamber, the results are valid before the flame front reaches the wall due to a negative impact of the chamber wall on the laminar flame propagation. It causes an energy loss of the burned gases to the wall and thus decreasing the rate of pressure rise. This negative effect is seen as the flame losing its spherical shape, becoming instable and wrinkling. A careful visual examination is conducted using the synchronized systems to consider a period from the flame onset up to the moment that either the flame front makes a contact with the wall or the cellular flames are initiated. The pressure-time data is then cropped up to this point for post-processing data analysis. In addition, since the flame has high stretch rate in start of propagation, the data are considered for the laminar burning measurement from flame radii greater than 4 cm to ensure that the flame is unstretched and the flame front thickness is negligible [23]. It is also assumed that the initial mixture constituents for H_2-O_2-N_2/Ar combustion are described as follows:

$$\varphi\, H_2 + \frac{1}{2}\Big(\, O_2 + 3.76\, \big((1-\alpha)\, N_2 + \alpha\, Ar\big)\Big) \qquad (1)$$

2.3.1 Theoretical Model

A thermodynamic multi-shell model has been developed to calculate the laminar burning velocity using experimental dynamic pressure data initially introduced by Metghalchi and Keck [24]. This model mainly assumes that two specific burned and unburned gas regions are present in the combustion vessel, separated by a negligible thickness reaction layer as described schematically in Figure 3. Moreover, it is assumed that: (1) the burned and unburned gases behave like an ideal gas, (2) the burned gas region is thermodynamically in the chemical equilibrium state, (3) the properties of the unburned gas region are kept frozen, (4) the thermal gradient in the burned gas section is negligible, (5) the burned and unburned gases are compressed isentropically, (6) a uniform spatial pressure distribution is applied throughout the vessel, (7) a preheat zone (with negligible thickness of δ_{ph}) with variable temperature surrounds the core burned gases which is covered by the unburned gases with uniform temperature, (8) a thermal boundary layer (with thickness of δ_{wb}) divides the core unburned gases from the chamber wall, and (9) flame front is expanding spherically and smooth.

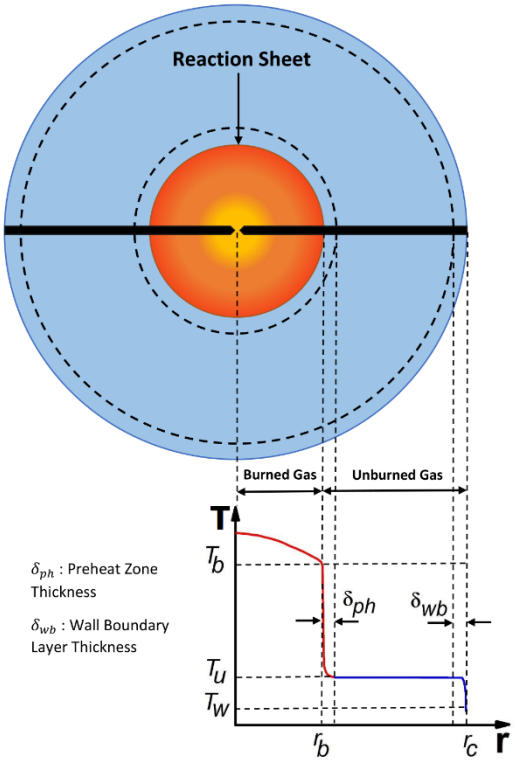

Figure 3: Schematic of thermodynamic multi-shell theoretical model

In a closed vessel, the spherical flame propagation is governed by conservation of mass and conservation of energy in mixture including the reaction layer and both burned and unburned gas

regions. According to mass balance equation for both burned and unburned gas section and taking account of the ideal gas equation of state, the total mass in the CVCC is defined as:

$$m_i = m_b + m_u = P_i(V_b + V_u)/RT_i \tag{2}$$

where the *m* and *V* represent the mass and volume of the gas mixture in a specific section, respectively, *P* and *T* are pressure and temperature within the CVCC, respectively, and *R* is the specific gas constant. The subscripts *i* is the initial conditions, while *b* and *u* represent the burned and unburned sections.

The volume of the gaseous mixture within the combustion chamber is as follows (v is specific volume of the gas mixture in a certain section):

$$V_i = \int_0^{m_b} v_b dm + \int_{m_b}^{m_i} v_u dm \tag{3}$$

The unburned gas region itself is divided into two specific segments: (1) a segment included in the thermal boundary layer of the chamber that transfer heat to the wall, (2) another segment that is far from the thermal boundary layer and compressed isentropically. Therefore, the second term of this equation is computed by the following equation where superscript ∞ represents the second segment with uniform temperature distribution:

$$\int_{m_b}^{m_i} v_u dm = \frac{R}{P}\int_{m_b}^{m_i} (T_u - T^{\infty}) dm + \int_{m_b}^{m_i} v_u^{\infty} dm \tag{4}$$

By changing the infinitesimal mass coordinate to a variable dependent to the chamber radius from the wall, and defining a displacement thickness concept (δ) [25] applied on the first term of this equation, the equation (3) can be rewritten as described below:

$$\delta = \frac{1}{\rho^{\infty}}\int_0^{\infty} (\rho_u - \rho^{\infty})\, dr \tag{5}$$

$$V_i + A\delta = \int_0^{m_b} v_b dm + \int_{m_b}^{m_i} v_u^{\infty} dm \tag{6}$$

where ρ is density in a specific region and *A* is combustion chamber wall area.

This equation is revised if divided by m_i:

$$\frac{V_i}{m_i} + \frac{A\delta}{m_i} = \int_0^{x} v_b dx' + \int_x^{1} v_u^{\infty} dx' \tag{7}$$

where x and x' represent the mass fraction of the burned gas section and integration variable, respectively.

In the view of conservation of energy, the energy equation for the gaseous mixture in the combustion chamber can be described as below:

$$E_i - Q = \int_0^{m_b} e_b\, dm + \int_{m_b}^{m_i} e_u\, dm \tag{8}$$

where e is specific internal energy in a specific region, E_i and Q are total initial energy and total energy conducted from the boundary layer displacement thickness to the combustion chamber wall, respectively.

Since the unburned gas region consists of two separate segments, the second term of this equation is calculated by:

$$\int_{m_b}^{m_i} e_u \, dm = C_v \int_{m_b}^{m_i} (T_u - T^{\infty}) \, dm + \int_{m_b}^{m_i} e_u^{\infty} \, dm \tag{9}$$

where C_v is the specific heat of unburned gas region at constant volume.

The energy balance equation is then summarized in the following format by changing the infinitesimal mass coordinate, defining a dependent variable to the chamber radius from the wall, and assuming one-dimensional heat conduction equation from the unburned gas region within the wall boundary layer to the chamber wall (δ' is integration variable in terms of δ):

$$E_i - A \int_0^{\delta} P \, d\delta' = \int_0^{m_b} e_b \, dm + \int_{m_b}^{m_i} e_u^{\infty} \, dm \tag{10}$$

This equation is revised if divided by m_i:

$$\frac{E_i}{m_i} - \frac{A}{m_i} \int_0^{\infty} P \, d\delta' = \int_0^{x} e_b \, dx' + \int_x^{1} e_u^{\infty} \, dx' \tag{11}$$

The two non-linear equations of (7) and (11) are required to be solved simultaneously to compute the mass fraction of the burned gas and temperature of the burned gas. Ultimately, the laminar burning velocity of spherical flames in the closed chamber can be defined by:

$$S_u = \dot{m}_b / \rho_u A_b = m \dot{x}_b / \rho_u^{\infty} A_b \tag{12}$$

In order to calculate the burned gases properties and all the thermodynamic properties of the mixture at local chemical equilibrium conditions, the numerical model is coupled with CANTERA package, an open-source chemical equilibrium code [26]. In addition, the thermodynamic data from JANAF (NASA) tables are utilized to quantify the unburned gas properties [27].

3. Results and Discussion

3.1 Flame morphological structure

Figure 4 displays the flame propagation snapshots of the H_2-O_2-N_2/Ar flames at an equivalence ratio of 0.2, two different initial pressures (0.2, 0.6 bar), an initial temperature of 298 K, and a flame radius of 55 mm for three different argon compositions in the mixture. These images implicitly show the effect of argon on the lean flammability limit of hydrogen combustion. The lean flammability limit of hydrogen at initial pressure of 0.2 bar can be extended in existence of 100% argon replaced for nitrogen; however, the mixture is not able to be ignited at 0% and 50% replacement. At an initial pressure of 0.6 bar, although argon addition leads to higher instability by generating cellular flames, it increases the burning velocity of the mixture. Furthermore, in cases with initial pressures of 0.6 bar, since equivalence ratio of 0.2 is the lower margin of the lean flammability limit of hydrogen combustion and burning velocities are slow, buoyancy effects

become significant [7]. The buoyancy effect causes the flame front to propagate more towards the top portion of the chamber. In addition, it was seen that the flame starts to quench in cases of α = 0% and α = 50% without developing too much in the lower portion of the CVCC.

Argon concentration (α)	α = 0%	α = 50%	α = 100%
Pi = 0.2 bar Φ = 0.2	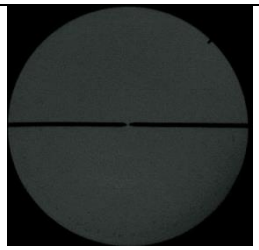	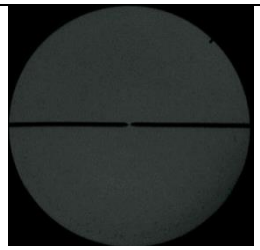	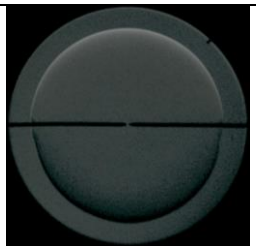
Time (ms)	-	-	61.25
Pi = 0.6 bar Φ = 0.2	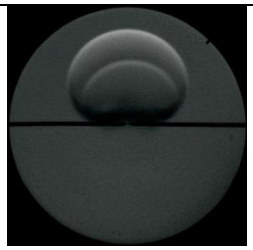	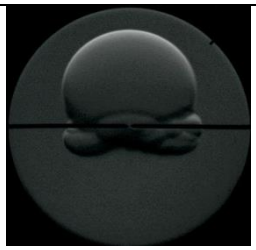	
Time (ms)	140.38	120.13	93.88

Figure 4: Snapshots of the H_2-O_2-N_2/Ar flames for lean flammability limit at initial pressures of 0.2, 0.6 bar and initial temperature of 298 K at flame radius of 55 mm

In Figure 5, the flame development images of H_2-O_2-N_2/Ar combustion for different flame radii are shown at initial pressure of 0.6 bar, equivalence ratios of 0.6 and 1.0, and different argon compositions. The flame front shows the formation of cracks at equivalence ratios of 0.6, 1, and 1.4 for all argon compositions; however, at an equivalence ratio of 0.6 and 0% argon replacement, cellular flame formation is also observed. The cases with equivalence ratios above 1.4 were observed with a smooth and laminar flame propagation.

Radius (mm)		15	35	55
Φ = 0.6	α = 0%	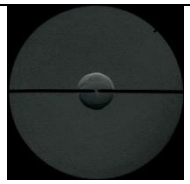	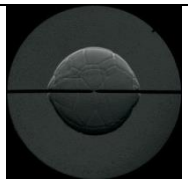	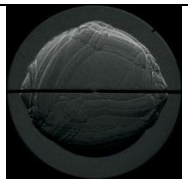
	Time (ms)	4.25	7.00	10.75
	α = 50%	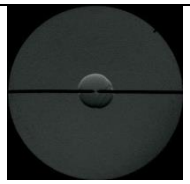	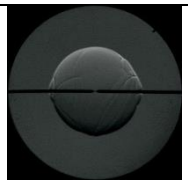	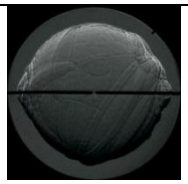
	Time (ms)	3.63	5.75	9.25
	α = 100%	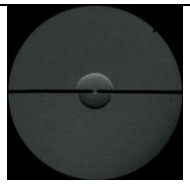	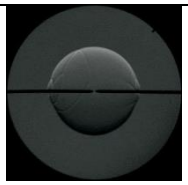	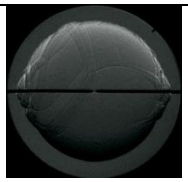
	Time (ms)	3.25	5.25	8.00

Φ = 1.0	α = 0%	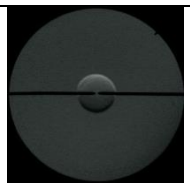	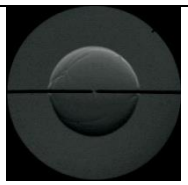	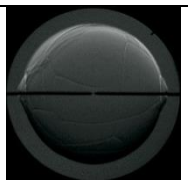
	Time (ms)	3.00	4.50	7.26
	α = 50%	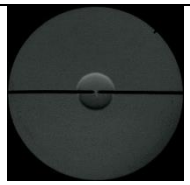	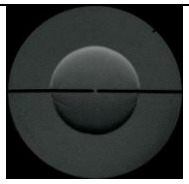	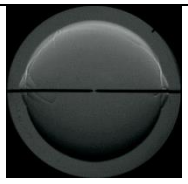
	Time (ms)	2.88	4.25	6.39
	α = 100%	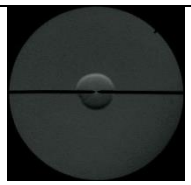	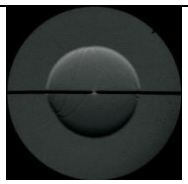	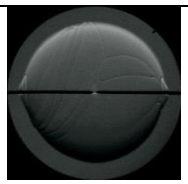
	Time (ms)	2.75	4.13	5.13

Figure 5: Snapshots of the lean and stoichiometric H_2-O_2-N_2/Ar flames for initial pressure of 0.6 bar and initial temperature of 298 K

3.2 Burning Velocity

Figure 6 shows the effect of equivalence ratio on laminar burning velocity of H_2-O_2-N_2/Ar flames for three different argon compositions. At an initial pressure of 0.2 bar, the mixture could not be ignited on equivalence ratios greater than 1.8 in which the highest laminar burning velocities for all cases are illustrated. Flame onset was observed in a wide range of equivalence ratios at initial pressure of 0.6 bar. The laminar burning velocity shows a negative parabolic behavior in terms of equivalence ratio for all argon compositions.

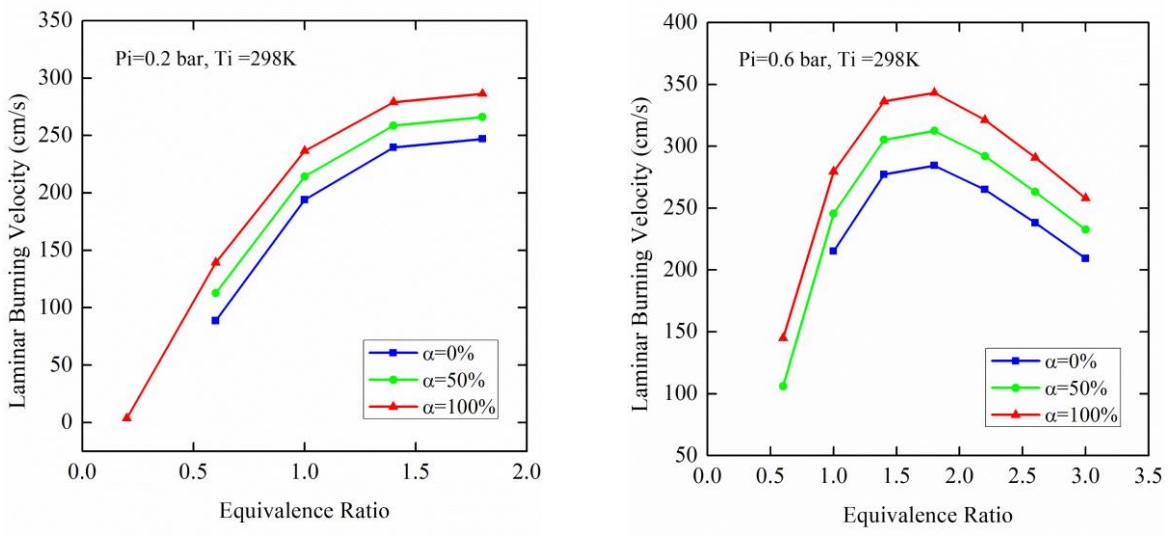

Figure 6: Effect of equivalence ratio on laminar burning velocity of H_2-O_2-N_2/Ar combustion for different argon concentrations

The effect of unburned gas temperature on laminar burning velocity of H_2-O_2-N_2/Ar combustion in terms of different argon compositions are presented in Figure 7. In all cases, a positive linear

dependency of unburned gas temperature on laminar burning velocity are observed. Moreover, since the flame was instable in some cases with an initial pressure of 0.6 bar and cellular flames were generated, the definition of laminar burning velocity (which assumes a smooth flame propagation) is only applied to a range of the data without the appearance of cellular flames.

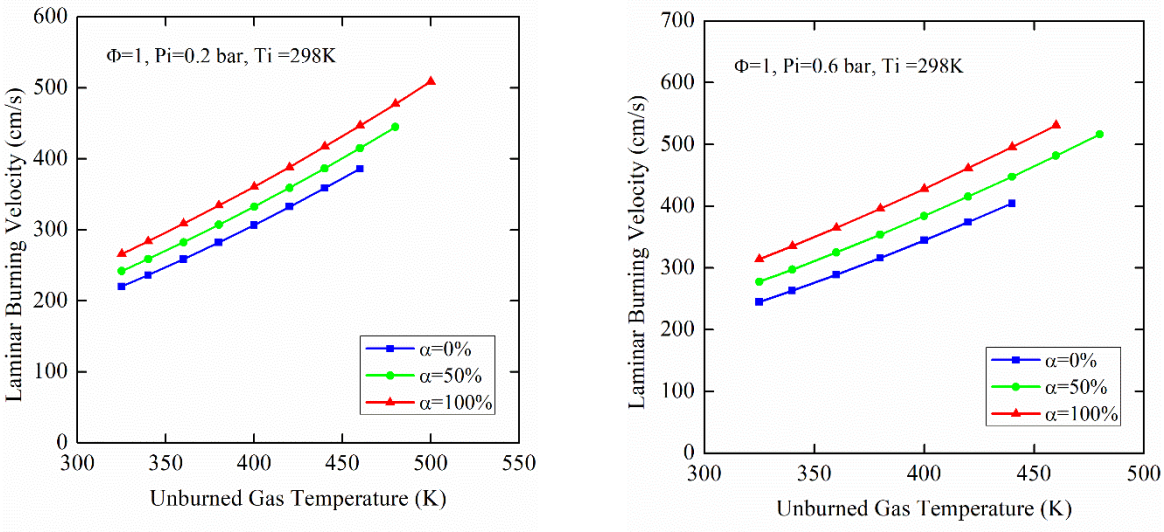

Figure 7: Effect of unburned gas temperature on laminar burning velocity of stoichiometric H_2-O_2-N_2/Ar flames for different argon concentrations

4. Conclusions

In this paper, the effect of argon as a working fluid on premixed hydrogen combustion in a constant volume combustion chamber has been studied. The outcomes of this study are as follows:

- Increasing argon concentration in the diluent mixture yields a positive dependency on the laminar burning velocity.
- Increasing argon in the mixture also yields an extension of the lean flammability limit of hydrogen at an initial pressure of 0.2 bar.
- At an equivalence ratio of 0.6 and an initial pressure of 0.6 bar, flame cracking and cellular flame formation are clearly observed.
- The laminar burning velocity at initial pressure of 0.6 bar showed a negative parabolic trend with the highest laminar burning velocity at equivalence ratio of 1.8.
- In all cases, increasing argon composition in the mixture led the higher laminar burning velocity at a specific equivalence ratio or a specific unburned gas temperature.
- At initial pressure of 0.2 bar, the mixture was not ignited at equivalence ratios above 1.8 and laminar burning velocity was only reported up to this equivalence ratio.

5. Acknowledgements

The authors would like to recognize the University of Massachusetts Lowell for supporting this research.

6. References

[1] S. O. Akansu, Z. Dulger, N. Kahraman, and T. N. Veziroğlu, "Internal combustion engines fueled by natural gas—hydrogen mixtures," *International Journal of Hydrogen Energy,* vol. 29, no. 14, pp. 1527-1539, 2004.

[2] R. J. Natkin, X. Tang, B. Boyer, B. Oltmans, A. Denlinger, and J. W. Heffel, "Hydrogen IC engine boosting performance and NOx study," SAE Technical Paper0148-7191, 2003.
[3] S. Mohsenian, M. S. Esmaili, J. Fathi, and B. Shokri, "Hydrogen and carbon black nano-spheres production via thermal plasma pyrolysis of polymers," *International Journal of Hydrogen Energy*, vol. 41, no. 38, pp. 16656-16663, 2016.
[4] Z. Yang *et al.*, "Investigation of Combustion Knock Distribution in a Boosted Methane-Gasoline Blended Fueled SI Engine," SAE Technical Paper0148-7191, 2018.
[5] B. Afkhami, A. Kakaee, and K. Pouyan, "Studying engine cold start characteristics at low temperatures for CNG and HCNG by investigating low-temperature oxidation," *Energy conversion and management*, vol. 64, pp. 122-128, 2012.
[6] M. Shahsavan, M. Morovatiyan, and J. H. Mack, "A numerical investigation of hydrogen injection into noble gas working fluids," *International Journal of Hydrogen Energy*, vol. 43, no. 29, pp. 13575-13582, 2018.
[7] D. B. Rhodes and J. C. Keck, "Laminar burning speed measurements of indolene-air-diluent mixtures at high pressures and temperatures," *SAE Transactions*, pp. 23-35, 1985.
[8] M. Shahsavan, M. Morovatiyan, and J. H. Mack, "A Computational Investigation of Non-Premixed Combustion of Natural Gas Injected into Mixture of Argon and Oxygen," in *ASME 2018 Internal Combustion Engine Division Fall Technical Conference*, San Diego, CA, 2018, p. V001T03A013: American Society of Mechanical Engineers.
[9] M. Morovatiyan, M. Shahsavan, M. Shen, and J. H. Mack, "Investigation of the Effect of Electrode Surface Roughness on Spark Ignition," in *ASME 2018 Internal Combustion Engine Division Fall Technical Conference*, San Diego, CA, 2018, no. 51982, p. V001T03A022, Volume 1: Large Bore Engines; Fuels; Advanced Combustion: American Society of Mechanical Engineers.
[10] L. M. Pickett, S. Kook, H. Persson, and Ö. Andersson, "Diesel fuel jet lift-off stabilization in the presence of laser-induced plasma ignition," *Proceedings of the Combustion Institute*, vol. 32, no. 2, pp. 2793-2800, 2009.
[11] B. Wolk, A. DeFilippo, J.-Y. Chen, R. Dibble, A. Nishiyama, and Y. Ikeda, "Enhancement of flame development by microwave-assisted spark ignition in constant volume combustion chamber," *Combustion and flame*, vol. 160, no. 7, pp. 1225-1234, 2013.
[12] M. Darzi, D. Johnson, C. Ulishney, and N. Clark, "Low pressure direct injection strategies effect on a small SI natural gas two-stroke engine's energy distribution and emissions," *Applied Energy*, vol. 230, pp. 1585-1602, 2018.
[13] K. Poorghasemi, R. K. Saray, E. Ansari, B. K. Irdmousa, M. Shahbakhti, and J. D. Naber, "Effect of diesel injection strategies on natural gas/diesel RCCI combustion characteristics in a light duty diesel engine," *Applied Energy*, vol. 199, pp. 430-446, 2017.
[14] M. Ghazikhani, M. E. Feyz, and A. Joharchi, "Experimental investigation of the exhaust gas recirculation effects on irreversibility and brake specific fuel consumption of indirect injection diesel engines," *Applied Thermal Engineering*, vol. 30, no. 13, pp. 1711-1718, 2010.
[15] M. R. Boldaji, B. Gainey, and B. Lawler, "Thermally stratified compression ignition enabled by wet ethanol with a split injection strategy: A CFD simulation study," *Applied Energy*, vol. 235, pp. 813-826, 2019.
[16] J. Natarajan, T. Lieuwen, and J. Seitzman, "Laminar flame speeds of H2/CO mixtures: effect of CO2 dilution, preheat temperature, and pressure," *Combustion and flame*, vol. 151, no. 1-2, pp. 104-119, 2007.
[17] O. Askari, Z. Wang, K. Vien, M. Sirio, and H. Metghalchi, "On the flame stability and laminar burning speeds of syngas/O 2/He premixed flame," *Fuel*, vol. 190, pp. 90-103, 2017.
[18] E. Rokni, A. Moghaddas, O. Askari, and H. Metghalchi, "Measurement of Laminar Burning Speeds and Investigation of Flame Stability of Acetylene (C2H2)/Air Mixtures," *Journal of Energy Resources Technology*, vol. 137, no. 1, p. 012204, 2015.
[19] G. Beretta, M. Rashidi, and J. Keck, "Turbulent flame propagation and combustion in spark ignition engines," *Combustion and flame*, vol. 52, pp. 217-245, 1983.
[20] J. C. Keck, "Turbulent flame structure and speed in spark-ignition engines," in *Symposium (International) on Combustion*, 1982, vol. 19, no. 1, pp. 1451-1466: Elsevier.
[21] S. Menon and A. R. Kerstein, "Stochastic simulation of the structure and propagation rate of turbulent premixed flames," in *Symposium (International) on Combustion*, 1992, vol. 24, no. 1, pp. 443-450: Elsevier.
[22] S. Shy, P. Ronney, S. Buckley, and V. Yakhot, "Experimental simulation of premixed turbulent combustion using aqueous autocatalytic reactions," in *Symposium (International) on Combustion*, 1992, vol. 24, no. 1, pp. 543-551: Elsevier.

[23] Z. Chen, M. P. Burke, and Y. Ju, "Effects of compression and stretch on the determination of laminar flame speeds using propagating spherical flames," *Combustion Theory and modelling,* vol. 13, no. 2, pp. 343-364, 2009.

[24] M. Metghalchi and J. C. Keck, "Burning velocities of mixtures of air with methanol, isooctane, and indolene at high pressure and temperature," *Combustion and flame,* vol. 48, pp. 191-210, 1982.

[25] M. Metghalchi, "Laminar burning velocity of mixtures of air with indolene, isooctane, methanol and propane," Massachusetts Institute of Technology, 1980.

[26] D. G. Goodwin, R. L. Speth, H. K. Moffat, and B. W. Weber, "Cantera: An object-oriented software toolkit for chemical kinetics, thermodynamics, and transport processes," Version 2.4.0 ed, 2018.

[27] J. Malcolm W. Chase, *NIST-JANAF Thermochemical Tables* (Washington, DC; New York :American Chemical Society; American Institute of Physics for the National Institute of Standards and Technology). 1998.